

## **Distribution Agreement**

In presenting this thesis as a partial fulfillment of the requirements for a degree from Emory University, I hereby grant to Emory University and its agents the non-exclusive license to archive, make accessible, and display my thesis in whole or in part in all forms of media, now or hereafter now, including display on the World Wide Web. I understand that I may select some access restrictions as part of the online submission of this thesis. I retain all ownership rights to the copyright of the thesis. I also retain the right to use in future works (such as articles or books) all or part of this thesis.

Joshua Pughe Sanford

March 25, 2017

Properties of Quantum Walks within Various One Dimensional Media

by

Joshua Pughe Sanford

Stefan Boettcher  
Adviser

Department of Physics

Stefan Boettcher  
Adviser

Bree Ettinger  
Committee Member

Jed Brody  
Committee Member

2017

Properties of Quantum Walks within Various One Dimensional Media

By

Joshua Pughe Sanford

Stefan Boettcher

Adviser

An abstract of  
a thesis submitted to the Faculty of Emory College of Arts and Sciences  
of Emory University in partial fulfillment  
of the requirements of the degree of  
Bachelor of Sciences with Honors

Department of Physics

2017

## Abstract

### Properties of Quantum Walks within Various One Dimensional Media

By Joshua Pughe Sanford

Recent work has shown that the canonical interpretation of Renormalization Group (RG) analysis on the quantum ultra walk produces incorrect results for determining the walk dimension, which describes the long term scaling of the system. Motivated by this inconsistency, we develop two numerical methods for approximating the walk dimension for 1D quantum walks. First, we approximate the walk dimension using the  $N^{\text{th}}$  moment of position in the large  $N$  limit. Then, we reproduce the walk dimension through envelope collapse.

These methods are used to compare the quantum ultra walk to its classical analog, the persistent random walk. These methodologies are then extended to the quantum random walk, as well as various walks with three chiral states, including the Grover walk, the cyclic Grover Walk, and the hierarchical Grover walk, all of which provide insight into the efficacy of our numerical methods as well as impart some understanding of how lattice geometry affects the scaling of the walk.

Though our analysis, it is found that both methods are widely applicable, yet become less accurate for walks with large coin variability relative to system size. Finally, we discuss how these methods can be made more robust, and conclude that, from the results of our numerical methods, the canonical interpretation of the RG flow for the quantum ultra walk is indeed misguided.

Properties of Quantum Walks within Various One Dimensional Media

By

Joshua Pughe Sanford

Stefan Boettcher

Adviser

A thesis submitted to the Faculty of Emory College of Arts and Sciences  
of Emory University in partial fulfillment  
of the requirements of the degree of  
Bachelor of Sciences with Honors

Department of Physics

2017

## Acknowledgements

I have been so lucky in my life to have friends, family, and professors that support me. While thanking them all would be of thesis length in its own right, I would like to give mention to a few key people who have supported me in this process.

First, I would like to thank Stefan Boettcher for his guidance and mentorship. Writing this thesis has been an incredibly enriching experience for me, and he made that possible. I would also like to thank Jed Brody and Bree Ettinger, both of whom served on my committee, but more importantly, both of whom have been influential to my growth as a student. I have learned so much from all of you.

Also, I would like to thank Asher Mouat for not only proofreading my thesis, but for spurring me on with coffee and supporting me with his company in my final hour. Similarly, I would like to thank Lindsay Rhoades for sitting in on my defense and being so supportive even though it made her late to her classes that day. To both of you: it meant a lot.

Lastly, I would like to thank my family. Their incredible support of me, both financially and emotionally, has never wavered. It is through their support that I was able to accomplish this. Love you guys.

## Table of Contents

I.	Introduction	1
II.	Structure of the One Dimensional Quantum Walk	2
	A. Walk Dimension	2
	B. Two State Walker, $n = 2$	2
	1. Delta Function Barriers, $n = 2$	2
	2. Random Quantum Walk, $n = 2$	3
	3. Ultra Walk, $n=2$	3
	4. Persistent Classical Walk, $n = 2$	3
	C. Three State Walker, $n = 3$	4
	1. Constant Grover Walk, $n = 3$	4
	2. Constant Cyclical Grover Walk, $n = 3$	4
	3. Hierarchical Cyclical Grover Walk, $n = 3$	4
III.	Modelling a Quantum Walk on a Classical Computer	4
IV.	First Passage Time within Delta Function Barriers	5
V.	Methods for Determining $d_w$	6
	A. Limiting Moments	6
	B. Determining $d_w$ through Scaling	6
VI.	Results of $d_w$ Finding Methods on Non-Ultra Walks	6
VII.	Conclusion	8

## Table of Figures

1	Visualization of Delta Barriers	3
2	Visualization of Ultra Barriers	3
3	Escape Time Result vs. Simulation	6
4	Inaccuracies of Low Moment Regression in Quantum Walks	6
5	Linearity of $\ln\langle x^N \rangle / N \ln t$ vs. $1/\ln t$ for Higher Moments of $x$	7
6	Comparison of PDFs between the Ultra Walk and the Persistent Classical Walk	7
7	Results of $d_w$ using the Limiting Moment Method	8
8	Results of $d_w$ using the Collapse Method	9
9	Results of $d_w$ for Derivatives of the Grover Walk	10
10	$d_w$ for the Quantum Random Walk	10
11	Comparison of Proposed Methods for Determining $d_w$	10

# Properties of Quantum Walks within Various One Dimensional Media

J. Pughe Sanford

Recent work has shown that the canonical interpretation of Renormalization Group (RG) analysis on the quantum ultra walk produces incorrect results for determining the walk dimension, which describes the long term scaling of the system. Motivated by this inconsistency, we develop two numerical methods for approximating the walk dimension for 1D quantum walks. First, we approximate the walk dimension using the  $N^{th}$  moment of position in the large  $N$  limit. Then, we reproduce the walk dimension through envelope collapse.

These methods are used to compare the quantum ultra walk to its classical analog, the persistent random walk. These methodologies are then extended to the quantum random walk, as well as various walks with three chiral states, including the Grover walk, the cyclic Grover Walk, and the hierarchical Grover walk, all of which provide insight into the efficacy of our numerical methods as well as impart some understanding of how lattice geometry affects the scaling of the walk.

Through our analysis, it is found that both methods are widely applicable, yet become less accurate for walks with large coin variability relative to system size. Finally, we discuss how these methods can be made more robust, and conclude that, from the results of our numerical methods, the canonical interpretation of the RG flow for the quantum ultra walk is indeed misguided.

## I. INTRODUCTION

The field of quantum walks (QW), in which the behavior of a wave function is studied as it evolves over a given system, has always shared a rich history with computer science. In the 80s, Richard Feynman developed a complete model for how a quantum computer could work, inspired in part by the principles of QW<sup>[1][2]</sup>. Shortly after, algorithms for such

a system began to circulate. Popularly referenced is Shor's algorithm<sup>[3]</sup> for prime factorization in polynomial time of  $\log n$ , which allows for RSA decryption to be brute forced in reasonable time frames. More relevant to our pursuits is Grover's search algorithm<sup>[4]</sup>, which utilizes a quantum cursor iterating over a complete graph to search for elements in  $\mathcal{O}(\sqrt{n})$  time complexity, significantly faster than its classical counterpart, the general number field

sieve. While many of these quantum mechanical algorithms do not require large system sizes to necessitate the rigorous study of dynamics, it is worthwhile to mention that any possible algorithm can be implemented as a quantum walk<sup>[5]</sup>. Where QW really find their motivation in computer science is in the study of how quantum computers may operate on sets of data. In other words, QW really find their motivation in studying the dynamics of how a quantum cursor will span the geometry of a data set.

The applicability of QW extend beyond the realm of computer science. In recent years, research has shown that many optical processes<sup>[6][7]</sup> can be modeled as QW, as well as various biological systems, such as that of photosynthesis<sup>[8][9]</sup>. Notably, these types of processes tend to occur on reasonably finite time scales ( $\sim 5$  discrete time steps in the photosynthetic cases), approximately the same order in length of walks being pioneered experimentally in the lab today<sup>[10][11]</sup>.

Many of the most sought after properties for computing purposes in QW tend to be asymptotic, such as hitting-time and mixing time, or the long term behavior of moments<sup>[12][13]</sup>. Many interesting journal pa-

pers have been written to date comparing these asymptotic limits to their classical counterpart <sup>[14][15]</sup>. One such asymptotic property that is crucial in understand the scaling of a quantum walk is its walker dimension,  $d_w$ , which describes the rate at which the walker spreads to other sites in time. Motivated in part by Grover's algorithm, researchers have found that the rate at which a walker traverses a lattice depends heavily on the geometry of the lattice itself. For example, in Grover's algorithm, speedup is achieved by enforcing the database to be a complete graph. By being able to quantify how the accessibility of sites scales with system size and system geometry, scientists can better develop architectures tailored to quantum computation.

The Renormalization Group treatment (RG) has been an effective approach to determining the scaling of many quantum and classical walks, when these walks are geometrically applicable<sup>[16][17][18]</sup>. RG utilizes the self similar structure of certain latices to iteratively derive long time scaling in the system. That is, by studying how the dynamics change with each rescaling, long term limits can be drawn from the system in ways that are relatively simple when compared to other methods. In

our study of this methodology, we have found that the canonical interpretation of the RG flow for the quantum ultra walk is inconsistent with numerically attained results. While the RG flow will not be discussed here, it will be used as a point of comparison for the numerical methods for determining  $d_w$  that we have developed here.

Motivated by this inconsistency, we hope to explore the scaling of the ultra-walk, attempting to understand how to best numerically reach the long term scaling limit for all such systems in which RG appears to fail. Using these methods, various other walks will also be explored as reference, including the persistent classical walk. Specifically, we will confine ourselves to the single particle walk on a 1D line. We first explore the QW between two delta function barriers, and move on from there to discuss: the ultra-walk, the persistent classical walk, the quantum random walk, the Grover walk, the cyclic Grover walk, and the hierarchical Grover walk.

Sec. II will discuss the structure of QW, as well as the exact formulation of each walk. Sec. III explains how these walks are formulated numerically. In Sec. IV, we discuss the first-passage time of a localized particle within

delta-function barriers, followed by Sec. II A, which describes the walk dimension,  $d_w$ . Finally, we discuss our results in Sec. VI and explore what to do next in Sec. VII.

## II. STRUCTURE OF THE ONE DIMENSIONAL QUANTUM WALK

The state of the quantum walker can be described entirely by the abstract vector  $|\Psi(t)\rangle$ . Over a 1D line composed of a discrete number of labeled sites,  $x$ , this description of walker can be decomposed along the position basis, resulting in

$$|\Psi(t)\rangle = \sum_{x=1}^N |x\rangle \langle x|\Psi(t)\rangle$$

Given an initial state  $|\Psi(0)\rangle$ , the evolution of this system is evolved by a unitary operator  $U$ , resulting in the master equation for discrete-time QW,

$$|\Psi(t + \tau)\rangle = U |\Psi(t)\rangle, \quad (1)$$

where  $\tau$  is the discrete time step. In our discussion of QW, we will treat  $t$  in units of  $\tau$ .  $U$  acts on  $|\Psi(t)\rangle$  at every site individually, directing the walker across the line from one site to the next. If only nearest neighbor and self interactions between sites are included,  $U$  can

be written in 1D as

$$U = \sum_x R_x |x+1\rangle \langle x| + L_x |x-1\rangle \langle x| + M_x |x\rangle \langle x|,$$

where  $R_x$ ,  $L_x$ , and  $M_x$  are the hopping operators at each position along the line, governing motion in the positive- $x$  direction, negative- $x$  direction, or stationary mixing, respectively. These operators act on  $|\Psi(t)\rangle$  both through mixing chiral states and through translating amplitude from one site to the next. As such, these operators can be written as the product of translation operators,  $T_{\{R,L,M\}}$ , and chiral mixing operators,  $C_x$  at each site. That is, the hopping operators can be written as,

$$\{R_x, L_x, M_x\} = T_{\{R,L,M\}} C_x.$$

The unitary requirement on  $U$ , such that the walker remains normalized, stipulates that

$$\begin{aligned} L_x^\dagger M_{x-1} + M_x^\dagger R_{x-1} &= \mathbf{0}, \\ L_x^\dagger R_{x-2} &= \mathbf{0}, \\ R_x^\dagger R_x + L_x^\dagger L_x + M_x^\dagger M_x &= \mathbb{I}_n, \end{aligned}$$

$n$  being the number of chiral states the walker can take on.  $R_x$ ,  $L_x$ , and  $M_x$  can be written as  $n \times n$  matrices whose size correspond to that of the  $n \times 1$  state vector.

## A. Walk Dimension

As previously alluded to, much interest lies in the asymptotic behavior of the quantum walk. A formal way of describing the asymptotic scaling of the probability distribution function (PDF) of a walk is through its dimension,  $d_w$ . It has been argued that classical walks conform to<sup>[19]</sup>

$$\rho(x, t) \sim t^{-\frac{d}{d_w}} f\left(\frac{x}{t^{\frac{1}{d_w}}}\right), \quad (2)$$

in the limit of  $t \rightarrow \infty$ , where  $d$  is the dimension of the lattice,  $d_w$  is the dimension of the walker, and  $f$  is Gaussian scaling function. Being 1D walks, all walks examined here have  $d = 1$ .

In quantum walks, this equation no longer holds, but does provide some guidance into what to expect. In the quantum case,  $f$  can no longer be considered Gaussian. That said, this formula guides in determining how to derive  $d_w$  from numerical results.

## B. Two State Walker, $n = 2$

For a two-dimensional walker, with right ( $\rightarrow$ ) and left ( $\leftarrow$ ) moving chiral states, we constrain  $M_x = \mathbf{0}$ , resulting in the canonical translational operators

$$T_R = \begin{pmatrix} 1 & 0 \\ 0 & 0 \end{pmatrix} \quad T_L = \begin{pmatrix} 0 & 0 \\ 0 & 1 \end{pmatrix},$$

which disregards all self-loops. Notice that, due to the duality in chiral states, the PDF of the walker at time  $t$  takes the form

$$\rho(x, t) = |\langle x | \Psi(t) \rangle|^2 = |\psi_{x,\rightarrow}(t)|^2 + |\psi_{x,\leftarrow}(t)|^2.$$

With that, we have a complete description of the geometry of the lattice. However, to fully define the system, the interaction of each node along the 1D line on the walker must also be defined. The coin set  $C_x$  is used to do so, directly governing the accessibility of each site. Three different unitary coin sets will be analyzed here, both using

$$C_x = \begin{pmatrix} \sin \theta_x & \cos \theta_x \\ \cos \theta_x & -\sin \theta_x \end{pmatrix}, \quad (3)$$

given a regime defining variable  $\theta_x \in \mathbb{R}$ .

### 1. Delta Function Barriers, $n = 2$

For  $\theta = \frac{\pi}{2}$ , Eq. 3 results in a fully transmissive coin. For  $\theta = 0$ , the coin becomes fully reflective. Thus, a free walker can be contained within two barriers situated at  $x = a$  and  $x = b$

simply by using the coin set

$$\theta_x = \frac{\pi}{2}(1 - \epsilon(\delta_{x,a} + \delta_{x,b})), \quad (4)$$

where  $\epsilon$  determines the leakage rate, or transmissivity, of the barriers. This coin set is visualized in Fig. 1.

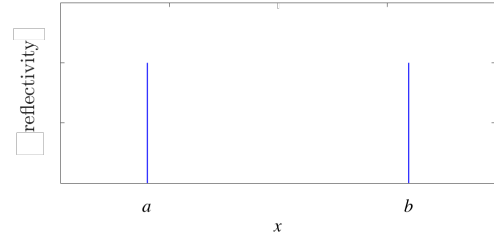


FIG. 1. Above is the Reflectivity of  $\theta_x$  vs.  $x$ . At sites  $a$  and  $b$ , the line has some  $\epsilon$ -dependent reflective component. Elsewhere, motion along the line is completely ballistic.

Being purely ballistic at all sites but  $x = a$  and  $x = b$ , the leading dynamics of this walk are determined by the interaction of the walker with the barriers. As a result of its simplicity, this walk provides for a straightforward understanding of how individual coins effect the walker.

### 2. Random Quantum Walk, $n = 2$

The random quantum walk is evaluated over the coin set,

$$\theta_x = \frac{\pi}{2}\omega_x, \quad (5)$$

were  $\omega_x$  is a randomly distributed variable  $\omega_x \in [0, 1]$ .

This coin set in an example of complete disorder, wherein properties are derived through the mean behavior of many walks as opposed to the behavior of just one. RG is not applicable to such a disordered model, forcing more rigorous analytical approaches to be taken. Konno<sup>[20]</sup> provides a very thorough analysis of this walk for

$$C_x = \frac{1}{\sqrt{2}} \begin{pmatrix} e^{2\pi i \omega_x} & 1 \\ 1 & -e^{-2\pi i \omega_x} \end{pmatrix}, \quad (6)$$

in which he proves that

$$\sum_{x=a}^b \rho(x, t) = \int_a^b \frac{1}{\pi(1-x^2)\sqrt{1-2x^2}} dx, \quad (7)$$

for symmetric, random distributions. Such a distribution (that is, time independent) indicates that the walk reaches a state at which scaling stops, i.e. the walker localizes with  $1/d_w = 0$ .

### 3. Ultra Walk, $n = 2$

The first order approximation of a completely disordered system is one with some type of geometry reducing symmetry. One very relevant example of such a system is the ultra walk. For the ultra walk, we'll de-

fine a coin space which is self-repeating in a hierarchical manner, one in which the distance between barriers of varying magnitude is ultrametric. In order to define such a coin space, we must first partition  $x$  into  $i$  sets that span the 1D line over the index  $j$ . Thus, we define

$$x_{i,j} = 2^i(2j + 1). \quad (8)$$

With this partition, we can construct the ultrametric barriers using the coin space,

$$\theta_x = \frac{\pi}{4} \epsilon^i, \text{ for } 0 \leq \epsilon \leq 1. \quad (9)$$

A visualization of this coin space can be seen in Fig. 2. Because this structure is self similar for  $x \rightarrow 2x$  and  $i \rightarrow i - 1$ , it should be solvable using an RG-treatment.

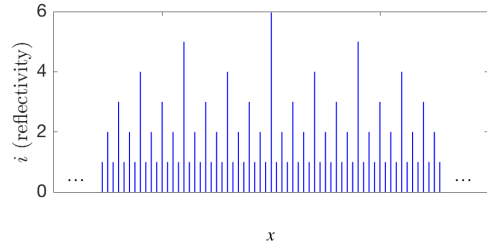


FIG. 2. Visualized above is  $i$  vs.  $x$ . This structure is self similar for  $x \rightarrow 2x$  and  $i \rightarrow i - 1$ . As a consequence, it's asymptotic behavior should lend itself to being solved using an RG treatment. However, this seems not to be the case.

$d_w$  for this geometry is not well studied, however, the endpoints of  $\epsilon$  are well known limiting cases. At  $\epsilon = 0$ , no amplitude escapes

from the origin, and  $1/d_w = 0$ , while at  $\epsilon = 1$  this becomes the Hadamard walk, resulting in  $1/d_w = 1$ .

#### 4. Persistent Classical Walk, $n = 2$

The persistent walk (PCW) is the closest classical analog to the quantum walk. The persistent walk is an extension upon the correlated random walk<sup>[21][22]</sup> in which the likelihoods of each chiral state at given moment depend upon all chiral states one moment before. This model will help us give footing to the quantum results, as classical walks have been more thoroughly studied to date.

What distinguishes the classical walk from the quantum walk is the restriction placed on  $U$ . In the quantum case,  $U$  must be unitary. However, in the classical walk, it needs to be a stochastic coin, where all rows and columns sum to unity. Thus, in a form analogous to the ultra QW, we define a coin set,

$$C_x = \begin{pmatrix} \theta_x & 1 - \theta_x \\ 1 - \theta_x & \theta_x \end{pmatrix}, \quad (10)$$

over the partition  $x_{i,j}$ , where again  $\theta_x = \frac{\pi}{4}\epsilon^i$  for consistency with the quantum ultra walk. This coin set results in a 1D line much like that in Fig. 2, but differs from the quantum

walk in notable ways. Notice that the PDF is no longer attained by the modulus of the wave function. Instead,

$$\rho(x, t) = \langle x | \Psi(t) \rangle = \psi_{x,\rightarrow}(t) + \psi_{x,\leftarrow}(t).$$

Another key difference is that at  $\epsilon = 1$ , this walk reduces to a biased random walk, resulting in  $d_w = 2$ , unlike  $d_w = 1$  for the quantum Hadamard case. More generally, RG treatment of this walk produces<sup>[23]</sup>

$$\frac{1}{d_w} = \begin{cases} 1 - \log_2 \epsilon, & \text{for } 0 < \epsilon < 1/2, \\ \frac{1}{2}, & \text{for } .5 \leq \epsilon \leq 1. \end{cases}$$

#### C. Three State Walker, $n = 3$

In the case of a three dimensional walker, we label its three chiral states right moving ( $\rightarrow$ ), left moving ( $\leftarrow$ ), and stationary ( $-$ ). In this definition, the probability distribution function (PDF) of the walker at time  $t$  takes the form

$$\begin{aligned} \rho(x, t) &= |\langle x | \Psi(t) \rangle|^2 \\ &= |\psi_{x,\leftarrow}(t)|^2 + |\psi_{x,-}(t)|^2 + |\psi_{x,\rightarrow}(t)|^2. \end{aligned}$$

Here we do not exclude  $M_x$ , such that the translational operators become

$$T_R = \begin{pmatrix} 1 & 0 & 0 \\ 0 & 0 & 0 \\ 0 & 0 & 0 \end{pmatrix}$$

$$T_L = \begin{pmatrix} 0 & 0 & 0 \\ 0 & 1 & 0 \\ 0 & 0 & 0 \end{pmatrix}$$

$$T_M = \begin{pmatrix} 0 & 0 & 0 \\ 0 & 0 & 0 \\ 0 & 0 & 1 \end{pmatrix}$$

We will look at various  $n = 3$  cases using these translational operators, with coin spaces all loosely based on the Grover coin.

1. *Constant Grover Walk,  $n = 3$*

For the Grover walk, we used a constant coin space,

$$C_x \equiv C^{(G)} = \frac{1}{3} \begin{pmatrix} -1 & 2 & 2 \\ 2 & -1 & 2 \\ 2 & 2 & -1 \end{pmatrix}. \quad (11)$$

It follows from the translational invariance of this system that  $d_w = 1$ .

2. *Constant Cyclical Grover Walk,  $n = 3$*

Further exploration was done into the  $n = 3$  case using the cyclical grover coin.

$$C_x \equiv C^{3(G)} = \frac{1}{3} \begin{pmatrix} 2 & 2 & -1 \\ 2 & -1 & 2 \\ -1 & 2 & 2 \end{pmatrix} = \begin{pmatrix} 0 & 0 & 1 \\ 1 & 0 & 0 \\ 0 & 1 & 0 \end{pmatrix}^{\frac{1}{2}}, \quad (12)$$

which will again result in  $d_w = 1$  due to translational invariance.

Notice that while the Grover coin is reflective, i.e.  $(C^{(G)})^2 = \mathbb{I}_3$ , the cyclical grover coin has a rotational group of 6, with  $(C^{3(G)})^6 = \mathbb{I}_3$ .

3. *Hierarchical Cyclical Grover Walk,  $n = 3$*

Finally, we attempted to create a model that mediated the ultra walk and the cyclical Grover walk by again partitioning the line with Eq. 8. Then we created the coin set,

$$C_x = \begin{pmatrix} 0 & 0 & 1 \\ 1 & 0 & 0 \\ 0 & 1 & 0 \end{pmatrix}^{\frac{1}{i+1}}. \quad (13)$$

This creates a hierarchical structure of cyclical coins, each in rotation group  $3(i + 1)$ .

While a rigorous derivation of  $d_w$  was not attempted for this walk, we will provide an intuitive argument as to why  $d_w$  should be one. Notice that  $\lim_{i \rightarrow \infty} C_x = \mathbb{I}_3$ . In other words, scaling this system as would be done in a rigorous RG treatment produces a self-similar structure that is effectively a constant line of  $\mathbb{I}_3$  coins. The translational invariance of this effective line results once again in  $d_w = 1$  for sufficiently large time scales.

### III. MODELLING A QUANTUM WALK ON A CLASSICAL COMPUTER

For all walks that do not contain fully reflecting sites or absorbing sites, there is guaranteed to be some finite amplitude at site  $\vec{\psi}_{\pm t}$  at time  $t$ . Thus, to simulate  $T$  units of time, a QW requires  $2T + 1$  sites in memory. Thus, let's define this as the system size  $N_T \equiv 2T + 1$ .

All data for the walk can then be placed in three matrices. There needs to be one  $n \times n \times N_T$  matrix,  $M$ , containing a coin for every site along the line, and two  $n \times N_T$  matrices to iterate the state of the walker over every time step, which we will label as  $S_a$  and  $S_b$ , containing the state of the system. Using a single matrix to store the state of the system would cause issues, as updating a single site requires the knowledge of both its neighbors one time step before, yet if either neighbor has already been updated, that information is lost. Thus, the initial condition can be stored in  $S_a$ , and  $S_a$  can then be operated upon, the result of which is stored in  $S_b$  and considered the current state. The subsequent iteration would then operate on  $S_b$ , storing the result in  $S_a$ , and so on.

Many architectures and class structures can be developed from here. In our implementa-

tion, we looked to optimize the runtime of the algorithm as much as possible, leading us to work in C++ with a few tweaks to the most basic algorithm. First, to minimize instantiation of some imaginary number class, we opted to create two versions of the state matrices, one of which stored the real component of the wave function,  $S_{a,r} = \text{Re}S_a$ , and one that stored the imaginary part,  $S_{a,i} = \text{Im}S_a$ . The properties of complex multiplication made this quite an easy partition to make. In our formulation of the coin space, we restricted all elements to the real numbers, and because of this no such distinction was needed.

To further aid element lookup, all matrices were made into row vectors. So, our coin matrix became a  $n^2 N_T \times 1$  vector, and our state matrices became  $n N_T \times 1$  vectors, which allowed all the elements of the original matrices to be appropriately mapped to elements in their respective vectors. By being selective with how that mapping occurs, it was possible to vectorize the loops such that many elements were adjacent in every loop. The exact details of this mapping depends on which walk was being modeled.

Certain techniques were consistently used to make sure the output was consistent with

the model. All QW use unitary coins, and as a consequence the normalization of the walker is conserved. We always used walkers with the initial condition (IC)  $|\psi_{\text{IC}}^{\vec{\alpha}}|^2 = 1$ . This allowed us not only to ensure unitarity of the coin set by checking that the norm of the wave function sums to unity, but also to monitor the drift in accuracy of the walk due to the limitations of machine accuracy. If all numerical results differ from the true value in some symmetric fashion, then the norm might still sum to unity, telling us nothing. However, when this value drifts from one, we can be sure that there are inaccuracies in the results. For our simulations, this result remained within  $10^{-8}$  units of 1 for system sizes on the order of  $N = 2^{22}$ . To accomplish this, we exploited the fact that numerical error stems mostly from summation rather than multiplication. As such, every sum was evaluated using the Kahan Summation Algorithm<sup>[24]</sup>.

Manual checks were made by placing the walker  $^T(1\ 0)$  at  $x = 0$  and comparing the first few iterations to those evaluated by hand. All further checks came on a case by case basis. For the ultra metric case, this meant reducing the model to something of known behavior and comparing the results. For the ultra walk,

$\epsilon = 1$  provides the well-studied Hadamard walk, for which results can be checked against. The Grover walk is similarly well published, and was able to be cross-checked that way.

It's worthwhile to mention that Eq. 5 is modeled on a calculator using a pseudo-random number generator. The generator was seeded using the start time of the simulation.

#### IV. FIRST PASSAGE TIME WITHIN DELTA FUNCTION BARRIERS

For the initial condition  $|\Psi(0)\rangle = \delta_{x,y}\delta_{\rightarrow}\psi_{\text{IC}}^{\vec{\alpha}}$ , for some  $y \in (a, b)$ , we can define the quantity

$$P_{\text{in}}(t) = \sum_{x \in [a, b]} \rho(x, t).$$

This quantity is invariant with respect to the evolution of the system for all moments in time at which no magnitude rests at the end points. Thus, for the coin set chosen, this means that, for some interval on the order of  $0 < t^* \leq (b - a)$ ,  $P_{\text{in}}(0) = P_{\text{in}}(t^*)$ . This, of course, depends on the chiral state and position of the initial walker along the line. This shows that when studying the first passage time of the walk beyond the region, all that matters is the amplitude at the boundary.

For our system, the subsequent time step past  $t^*$  results in interaction at the boundary, with

$$\begin{aligned} P_{\text{in}}(t^* + 1) &= |(R_a \vec{\psi}_a + L_b \vec{\psi}_b)|^2 \\ &\approx P_{\text{in}}(t^*) \cos^2 \frac{\pi}{2} (1 - \epsilon), \end{aligned}$$

depending on where  $\vec{\psi}_{\text{IC}}$  is placed in between the barriers. This relation is exact for IC at  $x = 0$ .

The reflected amplitude will traverse the interval until once again there exists amplitude at the interval's endpoints, which marks the exiting of amplitude across the barriers once more. In general, we can denote the number of times that the retained amplitude has completely returned to the barrier sites  $a$  or  $b$  as  $n$ . In our system, this is given by  $n = t/(b - a)$ . Given that no amplitude returns into the bounded region once escaped, the retained amplitude at iteration  $n$  can be generalized to

$$\begin{aligned} P_n &= \left| \left[ (R_a L_b)^{\frac{n}{2}} \begin{pmatrix} 1 & 0 \\ 0 & 0 \end{pmatrix} + (L_b R_a)^{\frac{n}{2}} \begin{pmatrix} 0 & 0 \\ 0 & 1 \end{pmatrix} \right] \vec{\psi}_{\text{IC}} \right|^2 \\ &= \cos^n \theta_a \cos^n \theta_b \left| \vec{\psi}_{\text{IC}} \right|^2. \end{aligned} \quad (14)$$

Using the symmetry of the coins at the barriers, this becomes  $P_n = P_0 \cos^{2n} \frac{\pi}{2} (1 - \epsilon)$ . We see from this simplification that the behavior

governing the escape of amplitude from delta function barriers is that of exponential decay. Utilizing our relation between  $n$  and  $t$ , we can write this as

$$P_{\text{in}} = P_0 e^{t/\mu}, \quad (15)$$

where  $\mu = (b - a)/2 \ln \cos \frac{\pi}{2} (1 - \epsilon)$ . This completely describes the partition of amplitude inside and outside of the barriers at time  $t$ . In other words, from this we can calculate how long it will take a given amount of amplitude to escape the barriers. Fig. 3 compares this formula to the numerically attained result.

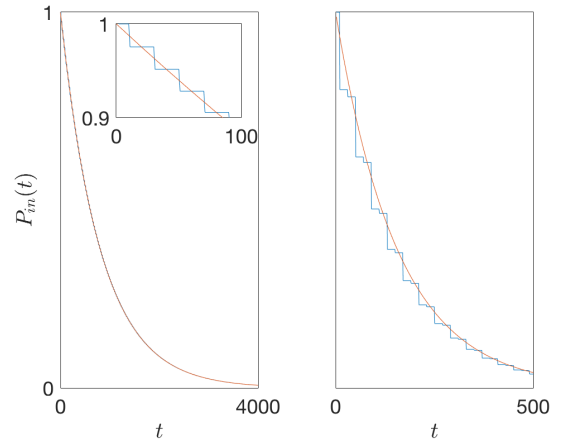


FIG. 3. Shown on the left is a comparison between Eq. 15 in orange and in the numerical result in blue, both for  $-a = b = 10$  and  $\epsilon = .9$ . In the overlay is the initial  $100\tau$  steps of the walk, which more accurately depicts the discrete nature of the walk which is not captured by Eq. 15. On the right is  $P_{\text{in}}(t)$  vs.  $t$  for asymmetric barriers, with  $\epsilon = .9$  at site  $x = a$  and  $\epsilon = .7$  at site  $x = b$ . While Eq. 15 no longer holds due to the asymmetry, Eq. 14 still captures the result accurately.

## V. METHODS FOR DETERMINING $d_w$

### A. Limiting Moments

Using Eq. 2, we can derive the  $N^{\text{th}}$  moment of  $x$  to be

$$\int dx x^N \rho(x, t) = t^{-\frac{1}{d_w}} \int dx x^N f\left(\frac{x}{t^{\frac{1}{d_w}}}\right)$$

$$\langle x^N \rangle = t^{\frac{N}{d_w}} \int d\mu \mu^N f(\mu),$$

such that

$$\frac{\ln \langle x^N \rangle}{N \ln t} \sim \frac{1}{d_w} + \frac{\ln A}{N \ln t}. \quad (16)$$

which holds for all  $N$  in the limit of  $t \rightarrow \infty$  for classic walks, where  $A = \int d\mu \mu^N f(\mu)$  and  $\mu = x/t^{1/d_w}$ . This equation is the motivation behind plotting  $\ln \langle x^2 \rangle / (2 \ln t)$  vs.  $1/\ln t$ , which intercepts the  $y$ -axis linearly at  $1/d_w$  in the classical case. By extrapolating numerical results,  $d_w$  can be found at  $t \rightarrow \infty$  with great accuracy. Given the effectiveness of this low moment approach classically, the naive next step would be to assume this relation holds in the quantum case as well. Fig. 4 shows this not to be the case. In QW,  $f$  is no longer guaranteed to be Gaussian. In the case of the ultra walk in particular,  $f$  manifests as a junction two regimes, one of which is governed by a power law in  $x$ , the other of which is an expo-

ponential falloff, as shown in Fig. 6. As a result,  $\ln A / \ln t$  is no longer well behaved for feasible simulation time scales  $t \sim 10^6 \tau$ , causing the the approach to  $d_w$  at  $t \rightarrow \infty$  to be nonlinear, confounding all extrapolative efforts. By taking the limit  $N \rightarrow \infty$  we are able to suppress the effects of  $\ln A / N \ln t$  on the approach to  $d_w$ , even for short time scales. The effects of this suppression can be seen in the lower plot of Fig. 5.

For the ultra walk,  $\ln A$  appears to have some dependency on  $N$ . This can be seen in Fig. 5, which shows the extrapolated value for  $d_w$  at  $t \rightarrow \infty$  as function of  $N$ . For large- $\epsilon$  the approach is linear, allowing for well fit extrapolation into  $N \rightarrow \infty$ . For low- $\epsilon$  however, there appears to be an  $\epsilon$ -dependent, dampened, oscillatory component that skews extrapolative efforts. Fig 7 shows the results for  $d_w$  using this method for various  $\epsilon$ .

### B. Determining $d_w$ through Scaling

A quick glance at Fig. 6 will suggest that the cutoff of the ultra walk scales with some power law of  $t$ . Eq. 2 supports this claim for classical walks, asserting that  $\rho(x, t)t^{(1/d_w)}$  collapses onto  $f$  for all  $t$ . Successful attempts have been made to extend this to quantum

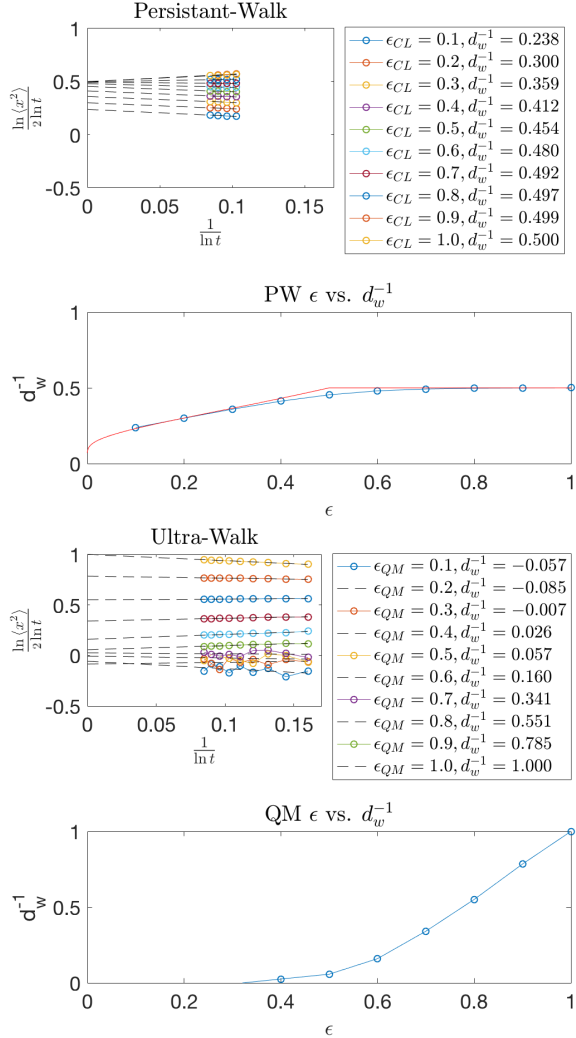


FIG. 4. Pictured above is the result of finding  $d_w^{-1}$  using equation Eq. 16 for  $t = 2^n \tau, n \in [10, 20]$ . Classically, this method works well, producing approximations that linearly approach there asymptotic value at  $t \rightarrow \infty$ , allowing for very accurate results of  $d_w$  using extrapolation. Moreover, the results produced by this method agree with the analysis of the persistent walk using RG (shown in red)<sup>[23]</sup>. In the quantum case, this only holds for  $\epsilon = 1$ , and becomes an increasingly incorrect approximation as  $\epsilon \rightarrow 0$ , where noisier PDFs create worse and worse numerical results over discrete times. We know with certainty the these results are incorrect in the low  $\epsilon$  range, as  $d_w$  becomes negative, which is not physical.

walks<sup>[16]</sup>, collapsing the PDFs of multiple time

steps onto  $f$  by scaling the  $x$  axis by  $t^{(1/d_w)}$ .

In our work, we determined the optimal value of  $d_w$  with which to collapse the PDFs by performing linear regression on the exponentially decaying tail of the cumulative distribution function (CDF) of the walk. We will label this region  $\mathbb{X}$ . To perform the regression, we defined

$$\Pi(x, t) = \int_{-\infty}^x \rho(x, t) dx.$$

Given that the tail of this CDF of an exponential curve is also exponential, linear regression can performed upon  $\log \Pi$  to find

$$\log \Pi(x, t_i) = \beta_1^{(i)} x + \beta_2^{(i)}, \text{ for } x \in \mathbb{X}_i.$$

Now, lets define  $\mathbb{Y}_i = \log \Pi(\mathbb{X}_i, t_i)$ . Upon scaling, CDFs for all time steps should collapse to the CDF of  $f$ . Thus, through scaling,  $\mathbb{Y}_i = \mathbb{Y}_j$  implies

$$\mathbb{X}_i t_i^{(1/d_w)} = \mathbb{X}_j t_j^{(1/d_w)}, \quad (17)$$

for all sufficiently large  $t$ . Therefore, we can define the algorithm as follows: given  $N$  unique time series and domains  $\{\mathbb{X}_i\}$  for a QW, we choose any given range  $\mathbb{Y}_R$  for  $R \in [1, N]$ . Using the results from the linear regressions,

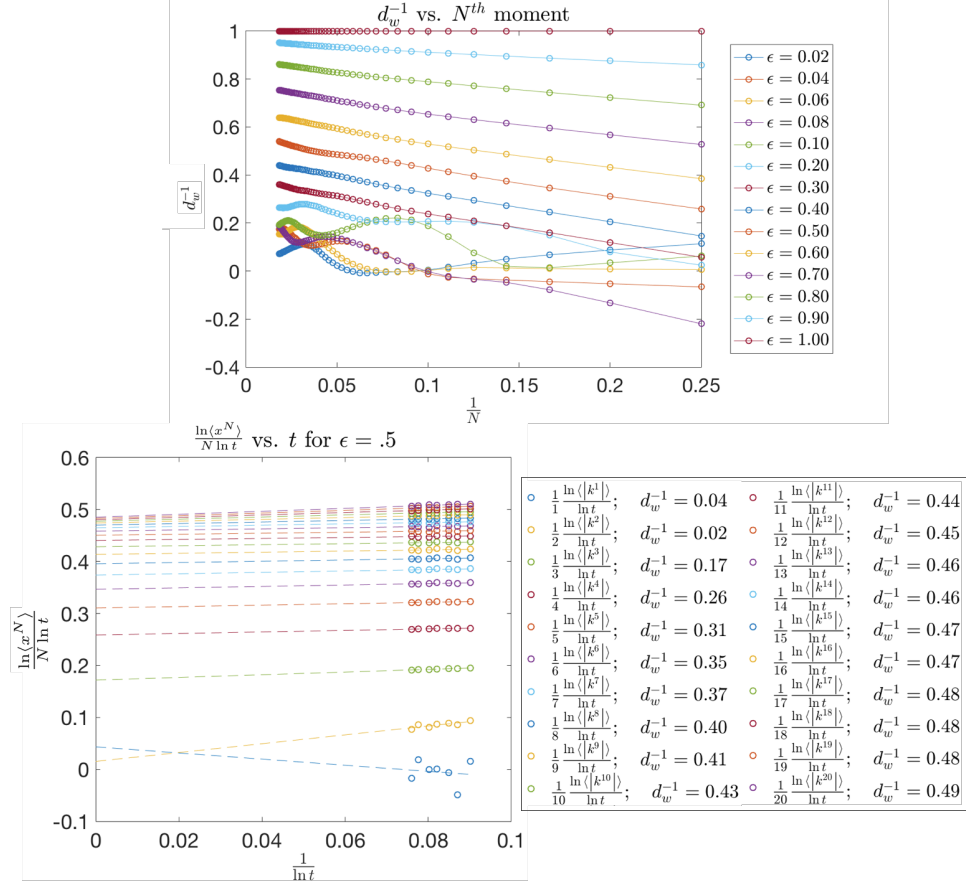


FIG. 5. Above (upper) is the result of finding  $d_w^{-1}$  using equation Eq. 16 for  $N \in [0, 55]$  and  $t = 2^{17}\tau$ . Using extrapolation, it is possible to find  $d_w^{-1}$  at  $N \rightarrow \infty$ . It is apparent that the approach  $\ln\langle x^N \rangle/N \ln t$  makes has some  $\epsilon$ -dependent oscillatory behavior and it appears that this oscillatory behavior is transient. Plotted below is the trajectory of  $d_w^{-1}$  vs.  $t$  for  $\epsilon = .5$ .

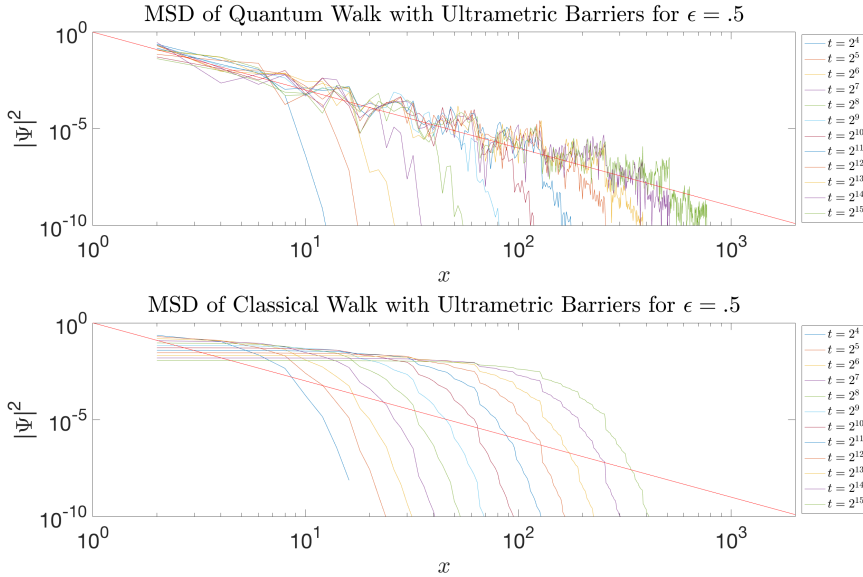


FIG. 6. To the left is a comparison of the PDF for QW vs. PCW. In the quantum walk, the envelope falls off like a power law, in this case  $x^{-3}$  (shown in red), until it reaches an exponential cut-off. This is not the case in the classical case, which is a scaled Gaussian distribution.

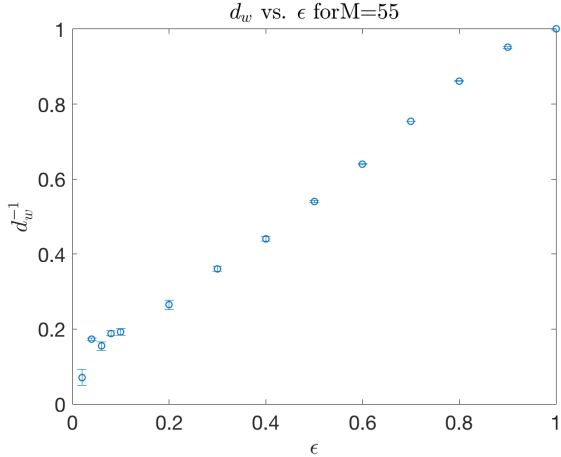


FIG. 7.  $d_w$  as determined by the relation  $\lim_{N \rightarrow \infty} \frac{\ln(x^N)}{N \ln t}$ . The method converges quickly for mid to high range  $\epsilon$ . However, machine accuracy did not allow for probing  $N > 55$ . As a result, the transient oscillatory behavior of the walks was still present for low- $\epsilon$ , leading to inaccurate results for  $d_w$ . Error bars were calculated using as the error in the y-intercept of our extrapolation on  $d_w$  over  $N$ .

determine new domains  $\{\mathbb{X}_i^* | \mathbb{X}_i^* = (\mathbb{Y}_R - \beta_2^{(i)}) / \beta_1^{(i)}\}$ , such that their ranges all equal  $\mathbb{Y}_R$ . At this point, Eq. 17 is true for all  $\mathbb{X}_i^*$  and  $\mathbb{X}_j^*$ . This now leaves you with  $N(N + 1)/2$  equations of the form

$$\frac{1}{d_w} = -\frac{\log(\mathbb{X}_i^*/\mathbb{X}_j^*)}{\log(t_j/t_i)},$$

for  $d_w$ . Figure 8 shows the results of this method over a range of  $\epsilon$  for the ultra walk.

## VI. RESULTS OF $d_w$ FINDING METHODS ON NON-ULTRA WALKS

Fig. 9 shows the results of the proposed methodologies for finding  $d_w$  in all three addressed Grover cases. Recall that  $d_w$  should tend to one in each of these cases. The limiting moment reaches a stable value almost immediately for both the Grover walk and the cyclic Grover walk. The hierarchical Grover walk does not converge completely to one, which can be attributed to us not probing far enough in time for the lattice to appear effectively constant. Also pictured in Fig. 9 is  $d_w$  as calculated using scaling over a variety of domains. Here we can see just how sensitive the scaling algorithm is to domain choice. The algorithm still finds values for  $d_w$  in the neighborhood of one, but not in a very distinguishable way. Had we not known what  $d_w$  to expect beforehand, this method could very easily produce some false value in the neighborhood of  $d_w$ . Further efforts will be focused around automating and optimizing the choice of domain such that the values for  $d_w$  produced by this method can be more reliable.

The numerical result of Konno's analytic result is produced in Fig. 10. Unfortunately, data was lost, restraining us to simply work-

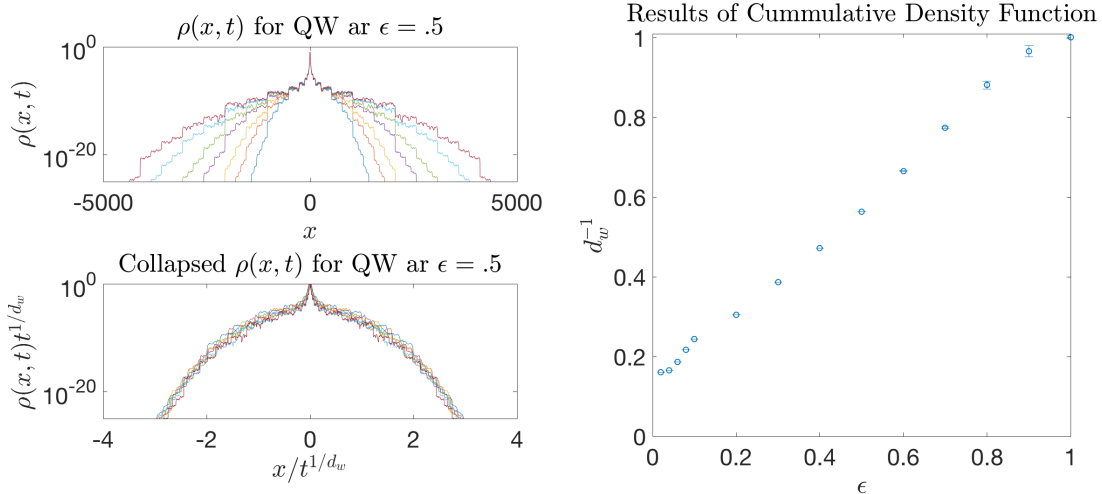


FIG. 8. On the left (upper) are the PDFs of the  $\epsilon = .5$  ultra walk at times  $t = 2^n$ ,  $n \in [10, 17]$ . Also left (bottom) are the PDFs once scaled by  $1/t^{1/d_w}$ . Both are smoothed using a 10 point moving average in order to show the mean curvature more clearly. On the right is the calculated result of  $d_w$  over  $\epsilon$ , including error bars. The error was calculated as the average root mean square error (RMSE) across all time series from the mean curvature,  $A$ . At lower  $\epsilon$ , it becomes harder to tell what the appropriate domains  $\{\mathbb{X}_i^*\}$  should be. As a result, human inaccuracies tend to skew  $d_w$  for lower values of  $\epsilon$ . This known source of error is not reflected in the magnitude of the RMSE for lower epsilon, indicating that RMSE might not be the best measure of error for this method.

ing with the second moment of the 500 walks simulated. However, even for  $N = 2$ , the second moment of the quantum random walk produces a result,  $d_w = 0.0395$ , fairly close to the one expected,  $d_w = 0$ .

## VII. CONCLUSION

Both methodologies for determining  $d_w$  proved successful, however, both procedures brought with them certain limitations. Taking the limiting moment is a robust method for many walks. However, it is not a viable method for walks that exhibit oscillatory behavior in  $d_w$ , as is the case in the ultra walk.

This is because this method relies on extrapolation to determine the  $N \rightarrow \infty$  limit, as machine precision limits us to much lower moments. The oscillatory behavior of certain walks skews the extrapolation results.

Similarly, the scaling approach to determining  $d_w$  also struggled in the low- $\epsilon$  regime, though it did so for different reasons. The downfall of this algorithm is that it depends heavily upon the choice of  $\{\mathbb{X}_i^*\}$ . These domains were especially hard to properly distinguish by eye in the low- $\epsilon$  regime, causing the algorithm to produce incorrect results with deceptively small variances. This algorithm would benefit greatly from automating

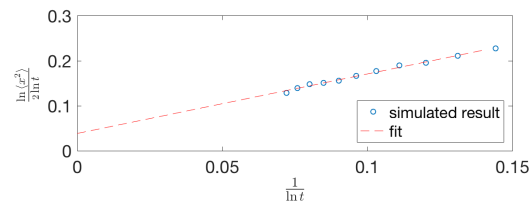
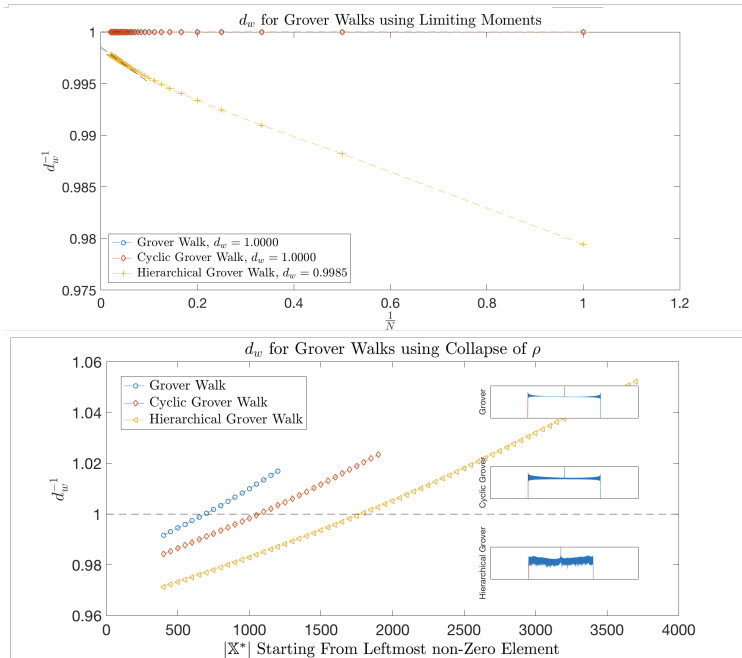


FIG. 10. Using moments to approximate the annealed envelope of  $N = 500$  random quantum walks at  $t = 2^n \tau$ ,  $n \in [1, 20]$ , it was found that  $d_w^{-1} \approx 0.0385$ . Due to the unfortunate loss of data, the ability to perform higher orders of  $N$  was lost, as was the opportunity to use scaling. Nonetheless, the random quantum walk appears relatively well for low moments.

FIG. 9. Results for the three Grover walks at  $t = 2^{17} \tau$ , using both limiting moments and linear regression. Plotted above is  $d_w$  for all moments  $N \in [1, 50]$ . All walks converge to approximately  $d_w = 1$ , as expected, with the hierarchical walk converging the slowest. Notice that the hierarchical walk does not converge to exactly one. For large enough scaling, the hierarchical matrix approaches the identity. Therefore,  $d_w$  should tend to one in the hierarchical Grover walk. This walk does not converge completely to one as  $N \rightarrow \infty$ , which can be attributed to us not probing far enough in time for the lattice to appear effectively constant. Below is  $d_w$  for each walk across for various numbers of sites used in the regression. That is, the x-axis describes the number of sequential sites used from the first non-zero site on the left. Inset on the plot is a depiction (all semi log plots) in red of the range used for each walk. Two take aways from this plot are how variable  $d_w$  is to the users choice of sites used in the regression, and that across all walk, the optimal number of sites seems to rest just below half of the exponentially falling reason.

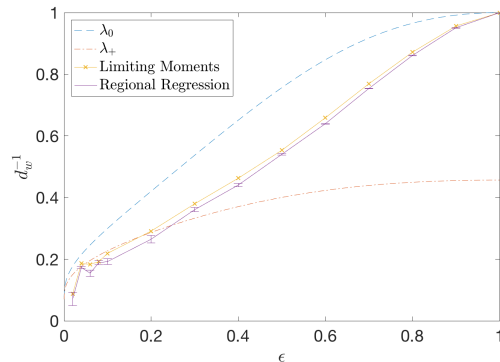


FIG. 11. Above is a comparison of the two proposed methods for determining  $d_w$ . This was done on the ultra walk over various  $\epsilon$  at  $t = 2^{17} \tau$ . Juxtaposed with our results are the two physical results for  $d_w$  derived by Boettcher and Faulkner using RG. As is made clear by this figure, the canonical interpretation of the RG flow is inconsistent with numerical methods.

the choice of  $\{\mathbb{X}_i^*\}$ . Notably, other forms of envelope collapse are possible, both through interpolation or higher order regression. While these methods were not explored here, they might prove helpful in lessening the sensitivity of this method on the choice of domain. This being said, the scaling approach is otherwise a robust method for determining  $d_w$ .

Plotted in Fig. 11 is a comparison of these results over  $\epsilon$ . Also shown in this plot are the two  $d_w$  parameters attained by RG analysis of the ultra walk<sup>[23]</sup>. Their analysis, which works perfectly for the PCW using ultra metric barriers, appears to fall apart for the quantum ultra case in light of the results we calculated

here. This begs the question, what interpretation of this RG flow accurately depicts the dynamics of the ultra walk, and what distinguishes the quantum ultra walk so uniquely from its peers? Something fundamental seems to set this walk apart from the others that have been studied. These unique features do not appear to effect the numerical collection of  $d_w$ , which allows the numerical methods developed here to act as a guide for the interpretation of RG analysis. Between improving these numerical methods and analytically solving the cyclic Grover walk, with its similar structure to that of the ultra walk, there remains much work to be done in fully understanding the scaling of ultra quantum walk.

- 
- [1] Richard P. Feynman. Quantum mechanical computers. *Foundations of Physics*, 16(6):507–531, June 1986.
  - [2] Richard Feynman. Simulating physics with computers. *International Journal of Theoretical Physics*, 21(6-7):467–488, June 1982.
  - [3] Peter W. Shor. Polynomial-Time Algorithms for Prime Factorization and Discrete Logarithms on a Quantum Computer. *SIAM Journal on Computing*, 26(5):1484–1509, 1997.
  - [4] Lov K. Grover. Quantum Mechanics helps in searching for a needle in a haystack, July 1997.
  - [5] Andrew Childs. Universal Computation by Quantum Walk. *Physical Review Letters*, 102(18):180501+, May 2009.
  - [6] Kia Manouchehri and Jingbo Wang. *Physical Implementation of Quantum Walks*. Springer Publishing Company, Incorporated, 2013.
  - [7] James G. Titchener, Alexander S. Solntsev, and Andrey A. Sukhorukov. Two-photon tomography using on-chip quantum walks. *Opt. Lett.*, 41(17):4079–4082, Sep 2016.
  - [8] Gregory S. Engel, Tessa R. Calhoun, Elizabeth L. Read, Tae-Kyu Ahn, Tomáš Mančal, Yuan-Chung Cheng, Robert E. Blankenship, and Graham R. Fleming. Evidence for wavelike energy transfer through quantum coherence in photosynthetic systems. *Nature*, 446(7137):782–786, April 2007.
  - [9] Masoud Mohseni, Patrick Rebentrost, Seth Lloyd, and Alan Aspuru-Guzik. Environment-assisted quantum walks in photosynthetic energy transfer. *The Journal of Chemical Physics*, 129(17):174106+, October 2008.
  - [10] A. Schreiber, K. N. Cassemiro, V. Potoček, A. Gábris, P. J. Mosley, E. Andersson, I. Jex, and Ch. Silberhorn. Photons walking the line: A quantum walk with adjustable coin operations. *Phys. Rev. Lett.*, 104:050502, Feb 2010.
  - [11] A. Schreiber, K. N. Cassemiro, V. Potoček, A. Gábris, I. Jex, and Ch. Silberhorn. Decoherence and disorder in quantum walks: From

- ballistic spread to localization. *Phys. Rev. Lett.*, 106:180403, May 2011.
- [12] Renato Portugal. *Quantum Walks and Search Algorithms*. Springer, 2013.
- [13] Salvador E. Venegas-Andraca. Quantum walks: a comprehensive review. *Quantum Information Processing* vol. 11(5), pp. 1015-1106 (2012), 2012.
- [14] Andrew M. Childs. On the relationship between continuous- and discrete-time quantum walk, April 2009.
- [15] Andrew M. Childs, Edward Farhi, and Sam Gutmann. An example of the difference between quantum and classical random walks. *Quantum Information Processing*, 1(1/2):35–43, March 2001.
- [16] Stefan Boettcher, Stefan Falkner, and Renato Portugal. Relation between random walks and quantum walks. *Phys. Rev. A*, 91:052330, May 2015.
- [17] A Maritan and A Stella. Exact renormalization group approach to ultradiffusion in a hierarchical structure. *Journal of Physics A: Mathematical and General*, 19(5):L269, 1986.
- [18] S Falkner S Boettcher and R Portugal. Renormalization group for quantum walks. *Journal of Physics: Conference Series* 473 (2013) 012018, 2013.
- [19] S. Havlin and D. Ben-Avraham. Diffusion in disordered media. *Advances in Physics*, 36(6):695–798, 1987.
- [20] Norio Konno. Quantum random walks in one dimension. 2002.
- [21] Eric Renshaw and Robin Henderson. The correlated random walk. *Journal of Applied Probability*, 18(2):403–414, 1981.
- [22] Anyue Chen and Eric Renshaw. The general correlated random walk. *Journal of Applied Probability*, 31(4):869–884, 1994.
- [23] Stefan Boettcher and Stefan Faulkner. Quantum ultra-walks: Walks on a line with spatial disorder. *unpublished*.
- [24] W. Kahan. Pracniques: Further remarks on reducing truncation errors. *Commun. ACM*, 8(1):40–, January 1965.